THE JOURNAL OF BIOLOGICAL CHEMISTRY VOL. 285, NO. 4, pp. 2554–2561, January 22, 2010
Printed in the U.S.A.

Crystal Structures of Progressive Ca^{2+} Binding States of the Ca^{2+} Sensor Ca^{2+} Binding Domain 1 (CBD1) from the CALX Na^+/Ca^{2+} Exchanger Reveal Incremental Conformational Transitions*

Received for publication, August 24, 2009, and in revised form, September 23, 2009 Published, JBC Papers in Press, October 8, 2009, DOI 10.1074/jbc.M109.059162

Mousheng Wu[‡], Hoa Dinh Le[§], Meitian Wang[¶], Vladimir Yurkov[§], Alexander Omelchenko[§], Mark Hnatowich[§], Jay Nix[‖], Larry V. Hryshko[§1], and Lei Zheng[‡2]

From the [‡]Center for Membrane Biology, Department of Biochemistry and Molecular Biology, the University of Texas Medical School at Houston, Houston, Texas 77030, the [§]Institute of Cardiovascular Sciences, St. Boniface Hospital Research Centre, University of Manitoba, Winnipeg, Manitoba R2H 2A6, Canada, the [¶]Swiss Light Source, Paul Scherrer Institute, CH-5232 Villigen, Switzerland, and the [‖]Molecular Biology Consortium, Advanced Light Source, Lawrence Berkeley National Laboratory, Berkeley, California 94720

Na^+/Ca^{2+} exchangers (NCX) constitute a major Ca^{2+} export system that facilitates the re-establishment of cytosolic Ca^{2+} levels in many tissues. Ca^{2+} interactions at its Ca^{2+} binding domains (CBD1 and CBD2) are essential for the allosteric regulation of Na^+/Ca^{2+} exchange activity. The structure of the Ca^{2+}-bound form of CBD1, the primary Ca^{2+} sensor from canine NCX1, but not the Ca^{2+}-free form, has been reported, although the molecular mechanism of Ca^{2+} regulation remains unclear. Here, we report crystal structures for three distinct Ca^{2+} binding states of CBD1 from CALX, a Na^+/Ca^{2+} exchanger found in *Drosophila* sensory neurons. The fully Ca^{2+}-bound CALX-CBD1 structure shows that four Ca^{2+} atoms bind at identical Ca^{2+} binding sites as those found in NCX1 and that the partial Ca^{2+} occupancy and apoform structures exhibit progressive conformational transitions, indicating incremental regulation of CALX exchange by successive Ca^{2+} binding at CBD1. The structures also predict that the primary Ca^{2+} pair plays the main role in triggering functional conformational changes. Confirming this prediction, mutagenesis of Glu^{455}, which coordinates the primary Ca^{2+} pair, produces dramatic reductions of the regulatory Ca^{2+} affinity for exchange current, whereas mutagenesis of Glu^{520}, which coordinates the secondary Ca^{2+} pair, has much smaller effects. Furthermore, our structures indicate that Ca^{2+} binding only enhances the stability of the Ca^{2+} binding site of CBD1 near the hinge region while the overall structure of CBD1 remains largely unaffected, implying that the Ca^{2+} regulatory function of CBD1, and possibly that for the entire NCX family, is mediated through domain interactions between CBD1 and the adjacent CBD2 at this hinge.

The Na^+/Ca^{2+} exchanger (NCX)[3] plays an important role in eukaryotic Ca^{2+} homeostasis. This transporter functions as a Ca^{2+} efflux mechanism across cell membranes and broadly participates in Ca^{2+}-mediated cellular signaling. NCXs have been identified in numerous tissues and cell types from several different species. In cardiac muscle, NCX1.1 plays a critical role in transsarcolemmal Ca^{2+} efflux, an essential requirement for cardiac relaxation (1). In neuronal tissues, a variety of exchangers are intricately involved in the control of excitation-secretion signaling (2). Notably, all characterized mammalian Na^+/Ca^{2+} exchangers exhibit a common Ca^{2+}-dependent regulatory mechanism, whereby their activity requires the presence of low concentrations of Ca^{2+} on their intracellular surface, and their activity is augmented in parallel with elevated intracellular Ca^{2+} levels (3). This important regulatory property may permit the timely coupling of exchange function to alterations in intracellular Ca^{2+} concentrations to meet the continuous needs for overall Ca^{2+} balance.

The general similarities of exchange function and regulatory properties within the large NCX protein family are ascribed to their conserved structural arrangements: nine predicted transmembrane (TM) segments form the ion translocation pathway and a large loop of ~500 amino acid residues splits TM helix-5 and -6 on the intracellular side of the molecule (4). Ca^{2+}-dependent regulation is attributed exclusively to Ca^{2+} interactions on the intracellular loop (5). A pair of Ca^{2+} binding domains (CBD1 and -2), called CALX-β motifs, has been identified (6). Sequence analysis revealed that CBD1 has conserved Ca^{2+} binding sites throughout the NCX family, whereas greater sequence diversity and/or Ca^{2+} binding capabilities occurs in CBD2 (7, 27). Given that CBD1 exhibits a higher Ca^{2+} affinity than CBD2 (8), it has been suggested that CBD1 acts as the primary sensor in the pair of CBDs. Mutations of carboxylate residues at CBD1 result in a pronounced reduction of the affinity for functional Ca^{2+} regulation (9). The Ca^{2+}-bound structures of CBD1 of NCX1 have recently been determined by NMR, and more recently by x-ray crystallography (8, 11). The

* This work supported by grants from the American Heart Association (0830353N to L. Z.) and the Canadian Institutes of Health Research (to L. V. H.).

The atomic coordinates and structure factors (codes 3EAD and 3E9T) have been deposited in the Protein Data Bank, Research Collaboratory for Structural Bioinformatics, Rutgers University, New Brunswick, NJ (http://www.rcsb.org/).

[1] Supported by a Canada Research Chair.

[2] To whom correspondence should be addressed: 6431 Fannin St., Houston, TX 77030. Tel.: 713-500-6083; Fax: 713-500-0545; E-mail: lei.zheng@uth.tmc.edu.

[3] The abbreviations used are: NCX, Na^+/Ca^{2+} exchanger; CBD1, Ca^{2+} binding domain 1; TM, transmembrane; MES, 4-morpholineethanesulfonic acid.

crystal structures revealed that four Ca^{2+} ions bind at the end of a β-sandwich structure of CBD1. More recently, a detailed study by backbone NMR suggested that Ca^{2+} binding induces a selective conformational change of CBD1 limited to the residues in the binding site, whereas the core of the β-sandwich structure remains unaffected (12). These observations raise a fundamental question of how the primary sensor role of CBD1 is conducted to the TM segments to control exchange activity.

There is currently no structure available for the apoform of CBD1. Consequently, there is no related mechanistic information or insight into how Ca^{2+} binding induces the conformational change of CBD1 required for transduction of this signal. In the reported Ca^{2+}-bound NCX1-CBD1 crystal structure, the Ca^{2+} binding site was saturated with four Ca^{2+} atoms (11). Whether these four Ca^{2+} access the binding site of CBD1 simultaneously or in a sequential way is unknown. Information of this type is critical toward understanding whether exchange function is simply switched on or off by Ca^{2+} or whether various degrees of exchange function are graded by different levels of Ca^{2+} occupancy.

CALX, a Na^+/Ca^{2+} exchange protein, was first identified in *Drosophila* photoreceptor cells (6, 13, 24). CALX is responsible for extruding intracellular Ca^{2+} from these cells and plays an essential role in light-mediated signaling in *Drosophila* sensory neurons (14). CALX shares 49% amino acid identity with the prototypical canine Na^+/Ca^{2+} exchanger, NCX1.1. Functionally, it shares many properties found in mammalian exchangers (13). However, CALX exhibits a completely opposite response to regulatory Ca^{2+} compared with all other characterized mammalian NCX homologs: the highest activity of CALX occurs in the complete absence of regulatory Ca^{2+} and its activity is progressively inhibited, rather than stimulated, by elevations in intracellular regulatory $[Ca^{2+}]$. This negative Ca^{2+} regulation of CALX leads to a considerable loss of signal amplification in the light response of the *Drosophila* visual system that triggers the photoreceptor cell cascade (14). CALX also possesses a pair of CBD domains on its intracellular loop. The mechanism underlying the negative Ca^{2+} regulatory phenotype observed for CALX is still elusive and enigmatic based on the existing structural information for NCX1. Our recent crystal structure of CALX-CBD2 showed that this site is not a functional Ca^{2+} binding site, suggesting that CBD1 must be the critical site involved in Ca^{2+} regulation of CALX (7). Furthermore, structural predictions, together with previous mutagenesis studies (7, 15) have strongly suggested that CALX-CBD1 possesses a similar Ca^{2+} binding site as does NCX1. To gain further insight into the Ca^{2+}-binding mechanisms of Na^+/Ca^{2+} exchange proteins in atomic detail and to investigate the negative Ca^{2+} regulatory property of CALX, we have determined crystal structures of CBD1 from CALX1.1 in the presence and absence of Ca^{2+} and studied the properties of this regulatory mechanism by mutagenesis and electrophysiology.

EXPERIMENTAL PROCEDURES

Expression and Purification of CALX-CBD1 Domains—The gene fragments encoding the CBD1 (amino acids 442–554) from a full length cDNA of *Drosophila* CALX1.1 were cloned into the vector pET28a (Novagen) with restriction sites of NdeI/XhoI. In the generated plasmid, CBD1 has an N-terminal His-tag spaced by a thrombin cleavage site. Protein expression was performed in *Escherichia coli* BL21(DE3) cells in the autoinduction medium (16) overnight at 25 °C. The cell pellet was suspended in a lysis buffer containing 50 mM sodium phosphate, 500 mM NaCl, 20 mM imidazole, pH 8.0, and ruptured by a high pressure homogenizer (Avestin). The lysate supernatant was applied to a nickel-nitrilotriacetic acid resin column (GE Healthcare), and the CALX-CBD1 protein was eluted with 300 mM imidazole. The purified protein was dialyzed overnight against a Tris-buffered saline buffer, pH 7.4, and was incubated with thrombin protease (GE Healthcare) overnight at 4 °C to truncate the His-tag. The proteolytic reaction mixtures were reapplied to nickel-nitrilotriacetic acid resin and the pass-through containing untagged CALX-CBD1 proteins was concentrated by Centricon (Millipore) and further purified by size-exclusion chromatography using a Superdex 75 10/300 GL column (GE Healthcare). The protein concentration was determined with a Coomassie protein determination kit (Pierce).

Crystallization of CALX-CBD1—All crystallization experiments were performed using the sitting-drop vapor diffusion method at 18 °C. CALX-CBD1, premixed with 1 mM $CaCl_2$ at a protein concentration of 10 mg/ml, was crystallized using the following conditions: 50 mM MES, pH 6.0, 20% polyethylene glycol 3350. To obtain the apoform crystals, CALX-CBD1 protein was incubated with 10 mM EDTA for 1 h and then dialyzed against Tris-buffered saline buffer, pH 7.4, prior to the crystallization experiment. The apoform crystals were obtained under different conditions using 100 mM Bis-Tris, pH 6.5, 200 mM NH_4Ac, 10 mM $MgCl_2$, 15% polyethylene glycol 10,000.

Data Collection—All crystals were flash-cooled to 100 K with 25% glycerol as the cryoprotectant. Diffraction data for the Ca^{2+} form crystal of CBD1 were collected at beamline X06SA of the Swiss Light Source (Villigen). A long wavelength (1.90 Å) was used for data collection with the intention of exploiting weak anomalous signals from Ca^{2+} atoms. The data collection for the apoform of CBD1 was carried out at the Advanced Light Sources beam line 4.2.2 (Berkeley, CA).

Data Processing and Structural Determination—Data processing, merging, and reduction were carried out with programs XDS and XSCALE (17). The CALX-CBD1 structures were solved using the molecular replacement method by the program PHASER (18) and using the CBD1 structure from NCX1 (Protein Data Bank code 2DPK) as a search model. Both structures were refined using the program Refmac (19). The model building was performed using COOT (20). Crystallographic data and the model refinement statistics are given in Table 1. The anomalous Fourier map in Fig. 1*A* was calculated using the program FFT (21) with phases from the final refined coordinates and observed anomalous difference in diffraction data. All figures were prepared using the program PyMOL (22).

Circular Dichroism (CD) Spectroscopy—Prior to CD spectroscopic analysis, CALX-CBD1 protein used for crystallization was passed through a desalting column (GE Healthcare) equilibrated with a solution containing 200 mM NaF, pH 7.4, to remove any Cl^-. The protein concentration was adjusted to 1 mg/ml before measurement. CD spectra of the CBD1 protein were collected at room temperature over a wavelength range

from 190 to 260 nm with a Jasco J-720 spectrometer using a 0.02-cm cylindrical cell.

Mutational Analysis Using Giant Excised Patch Clamping—Mutations of CALX1.1 were introduced by a modified site-directed mutagenesis procedure (23). To exclude the possibility of random PCR errors on large cNDA of CALX (>3 kb), a minimal DNA fragment containing the sequencing-confirmed mutations was recloned back to the parent vector with appropriate restriction sites.

The effect of each mutation on Ca^{2+} regulation of CALX1.1 was measured by outward Na^+-Ca^{2+} exchange current recordings using the giant, excised patch clamp technique, as described previously (24). Briefly, *Xenopus laevis* oocytes were injected with ~23–35 ng of cRNA of wild-type or mutant CALX1.1 and maintained at 18 °C. Electrophysiological measurements were typically obtained from day 3 to 7 postinjection. Borosilicate glass pipettes were pulled and polished to a final, inner diameter of ~20–30 μm, and coated with a Parafilm®:mineral oil mixture to enhance patch stability and reduce electrical noise. Oocytes were briefly (~5–10 min) transferred to a solution containing: 100 mM KOH, 100 mM K-aspartate, 100 mM MES, 20 mM HEPES, 10 mM NH_3SO_3, 5.0 mM EGTA, 5.0 mM $Mg(OH)_2$; pH 7.0, at room temperature (with MES) to allow sufficient shrinkage of the cells in order for their vitellin layers to be removed by dissection. Giga ohm seals were formed by gentle suction, and membrane patches were excised by progressive movements of the pipette tip. Rapid solution changes were introduced using computer-controlled, multi-channel perfusion devices. Axon Instruments® hardware and software were used for data acquisition. A holding potential of 0 mV was employed for all current measurements.

Pipette solutions contained 100 mM *N*-methyl-D-glucamine, 100 mM MES, 30 mM HEPES, 30 mM TEA-OH, 16 mM sulfamic acid, 8.0 mM $CaCO_3$, 6.0 mM KOH, 0.25 mM ouabain, 0.1 mM flufenamic acid, 0.1 mM niflumic acid; pH 7.0, at room temperature (with MES). Currents were elicited by switching from Li^+- to Na^+-based perfusion solutions containing: 100 mM NaOH or LiOH, 100 mM L-aspartic acid, 20 mM CsOH, 20 mM HEPES, 20 mM TEA-OH, 10 mM EGTA, 3.00–21.84 mM NH_3SO_3, 0–9.91 mM $CaCO_3$, 1.00–1.50 mM $Mg(OH)_2$; pH 7.0, at 30 °C (with MES or LiOH). Stock solutions of $CaCO_3$ and $Mg(OH)_2$ were prepared in a ratio of 1:2 with sulfamic acid. Total Mg^{2+} and Ca^{2+} were adjusted to yield free concentrations of 1.00 mM and 0–30 μM, respectively, using MAXC software (25).

All experiments were conducted at 30 °C. Origin® software was used for curve-fitting and statistical analyses. Pooled data are mean ± S.E. Student's *t* test or one-way analysis of variance and Tukey's post hoc test, were used for statistical determinations. $p < 0.05$ was considered significant.

RESULTS

Overview of CALX1.1-CBD1 Structure—The Ca^{2+}-bound structure of CALX-CBD1 was determined at 2.25 Å resolution. The structure shows CALX-CBD1 has an immunoglobulin-like conformation formed by two anti-parallel β-sheets consisting of β-strands, A, B, G and C, D, E, F, respectively (Fig. 1*A*). CALX-CBD1 shares 60% sequence identity with that of canine NCX1-CBD1. Consequently, these two structures can be superimposed with a root mean square deviation of 0.84 Å for 113 aligned Cα atoms. The most significant difference between these two CBD1 structures occurs within their F-G loops. CALX-CBD1 has a rather short F–G loop with only 9 residues, whereas its counterpart from NCX1 consists of 28 residues and displays high flexibility, as indicated in the NMR structure (8).

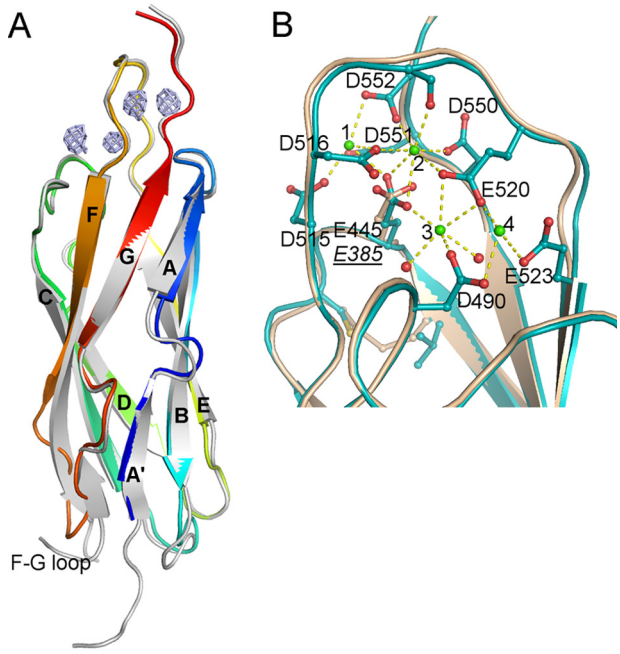

FIGURE 1. **Crystal structures of CALX-CBD1.** *A*, structural alignment of the CBD1 from CALX and NCX1. CALX-CBD1 shown as *rainbow ribbons* was superimposed on the NCX1-CBD1 crystal structure shown in *gray*. The anomalous difference map is displayed in slate and contoured at 6.0σ to indicate the Ca^{2+} positions. The short F–G loop of CALX is highlighted, whereas that from NCX1 is invisible. *B*, structural alignment of the Ca^{2+} binding sites of CALX-CBD1 and NCX1-CBD1. The Ca^{2+}-bound CALX-CBD1 structure in *cyan* is superimposed onto the NCX1-CBD1 structure (colored in *wheat*). Four Ca^{2+} and water molecules are represented as *green* and *red spheres*, respectively. The residues coordinating Ca^{2+} are shown as *stick balls*; Ca^{2+} interactions with residues are shown as *yellow dashed lines*. The label for the E385 residue in NCX1 is shown in *underlined italics*.

Ca^{2+} Binding Site of CALX-CBD1—The Ca^{2+}- bound CALX-CBD1 crystal diffraction data set was collected at 1.9 Å wavelength, allowing the assignment of the bound Ca^{2+} by examination of the anomalous signal (Fig. 1*A*). Four Ca^{2+} are clustered in the distal loops of the β-sandwich with ~4 Å equal distance spacing between them. Nine carboxylate residues are involved in the coordination of Ca^{2+} (Fig. 1*B*). The side chains of these acidic residues are arranged in a zipper-like orientation, forming an extensive carboxylate cluster at the top of this β-sandwich. The E–F loop is the major component in the Ca^{2+} binding site with five of its residues involved in Ca^{2+} coordination. That is, the E–F loop crosses over the Ca^{2+} zipper line clamping Ca-1, -2, and -3 ions through coordination with carboxylate groups of Asp^{515}, Asp^{516}, and Glu^{520} together with the carbonyl oxygen atoms of Asp^{517} and Val^{518}. Compared with Ca-1 or -2, which is penta- or hexacoordinated, Ca-4 is only tricoordinated with Asp^{490}, Glu^{523}, and Glu^{520}. Consequently, Ca-4 displays the highest thermal B factor, suggesting it may be the most mobile species during these ligand interactions.

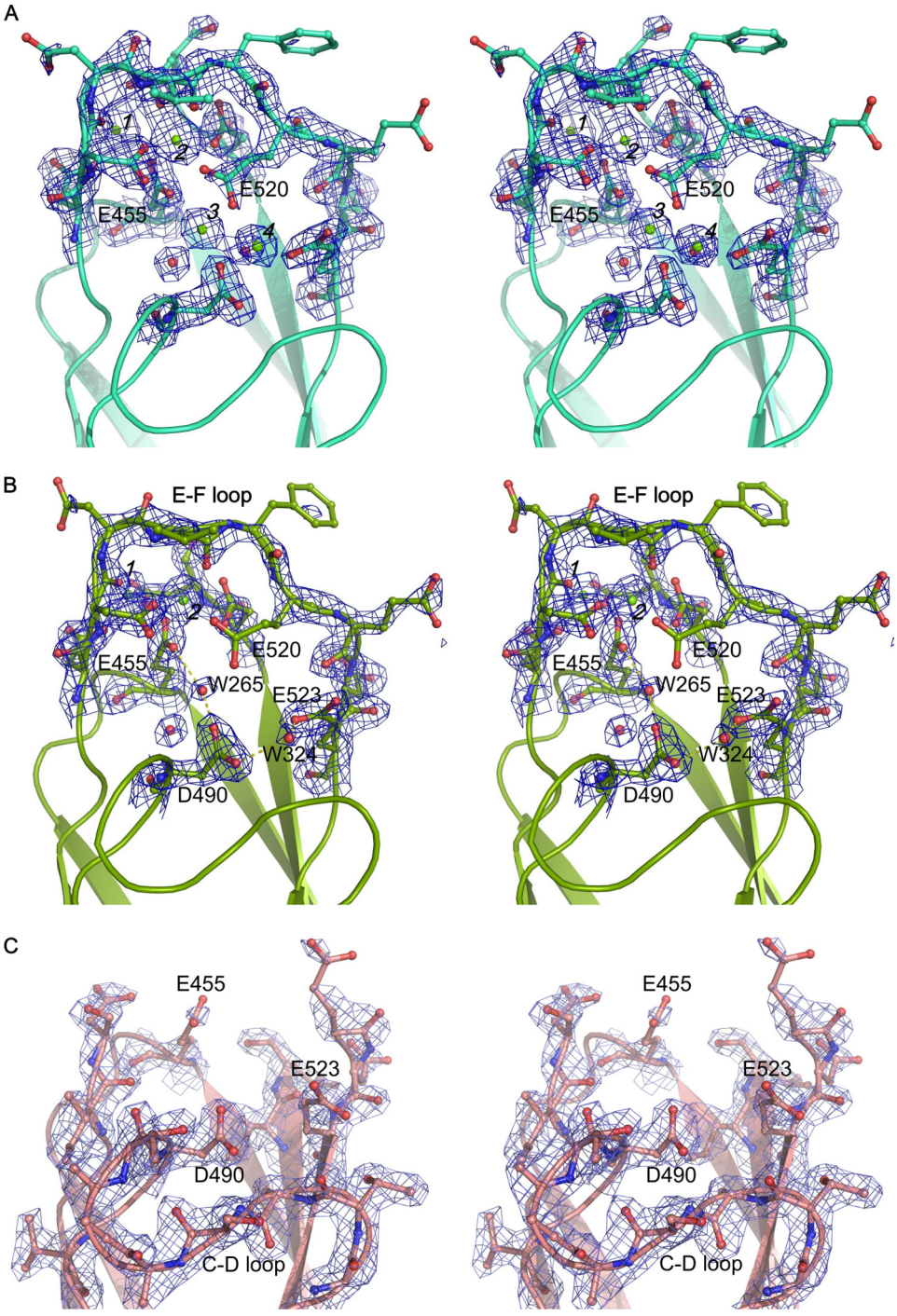

FIGURE 2. **Stereo views of conformational changes in the Ca^{2+} binding sites of CALX-CBD1.** $2F_o - F_c$ electron density maps contoured at 1.5σ level are shown in *blue*. Ca^{2+} and water molecules are represented as *green* and *red spheres*, respectively. The residues coordinating Ca^{2+} are shown as *stick balls*. Hydrogen bond interactions are shown as *yellow dashed lines*. *A*, *B*, and *C* represent three different conformations from the same asymmetric unit of the apoform CALX-CBD1 structure. *A*, monomer B (four Ca^{2+}-bound); *B*, monomer A (two Ca^{2+}-bound); and *C*, monomer C (no Ca^{2+}-bound).

The Ca^{2+} binding sites of CALX-CBD1 are almost identical to those of NCX1 except for Glu^{455}, which locates centrally on the basement of the binding site. Compared with the NCX1 structure, this residue rotates its carboxyl group by 90°, resulting in simultaneous coordination with three Ca^{2+} (Ca-1, Ca-2, and Ca-3) instead of one (Ca-2) shown in the NCX1-CBD1 structure (11). In addition, it appears that the disulfide bridge locking the A–B loop near Glu^{385} in the NCX1-CBD1 structure is absent in CALX-CBD1, as a valine replaces cysteine at position 453.

Conformational Change in the Apoform Structure—To gain additional structural information regarding Ca^{2+} binding to CBD1, the CBD1 protein was treated with 10 mM EDTA and dialyzed prior to crystallization; the apoform structure was determined at 1.6 Å resolution. The EDTA-treated sample gives the same crystal packing as that of the Ca^{2+}-bound form; four monomers assemble in anti-parallel in an asymmetric unit. The overall structure of the apoform CBD1 shows no overall conformational changes compared with the Ca^{2+}-bound form except within the Ca^{2+} binding sites. In the Ca^{2+}-bound structure, Ca^{2+} binding sites of four monomers in an asymmetric unit were identically and fully occupied. In contrast, the same binding sites exhibit three distinct Ca^{2+} binding states in the apoform structure. Monomer B shows a full occupancy state as shown in the Ca^{2+}-form structure, where four Ca^{2+} were found in the Ca^{2+} binding site and all residues involved in Ca^{2+} coordination are clearly visible (Fig. 2*A*).

However, monomer A displays a partial Ca^{2+} binding state. Only Ca-1 and -2 (the primary Ca^{2+} pair) were found at similar positions as in monomer B (Fig. 2*B*). The absence of Ca-3 and Ca-4 (named as the secondary Ca^{2+} pair) does not result in any significant structural change compared with monomer A with root mean square deviation values of 0.28 Å for backbone atoms and 0.68 Å for all atoms. The conformational change occurs exclusively at Glu^{520}, whose side chain is invisible in the electron density map. The backbone of the entire E–F loop is still clearly resolved and appears to be stabilized by the primary Ca^{2+} pair. However, the thermal B factors of the residues on the E–F loop are considerably increased compared with those in monomer B (Fig. 3). A water molecule at position 265 was found at Ca-3 position, which forms two hydrogen bonds with Glu^{455} and Asp^{490}. No density can be observed in the Ca-4 position. The conformations of Asp^{490} and Glu^{523} remain

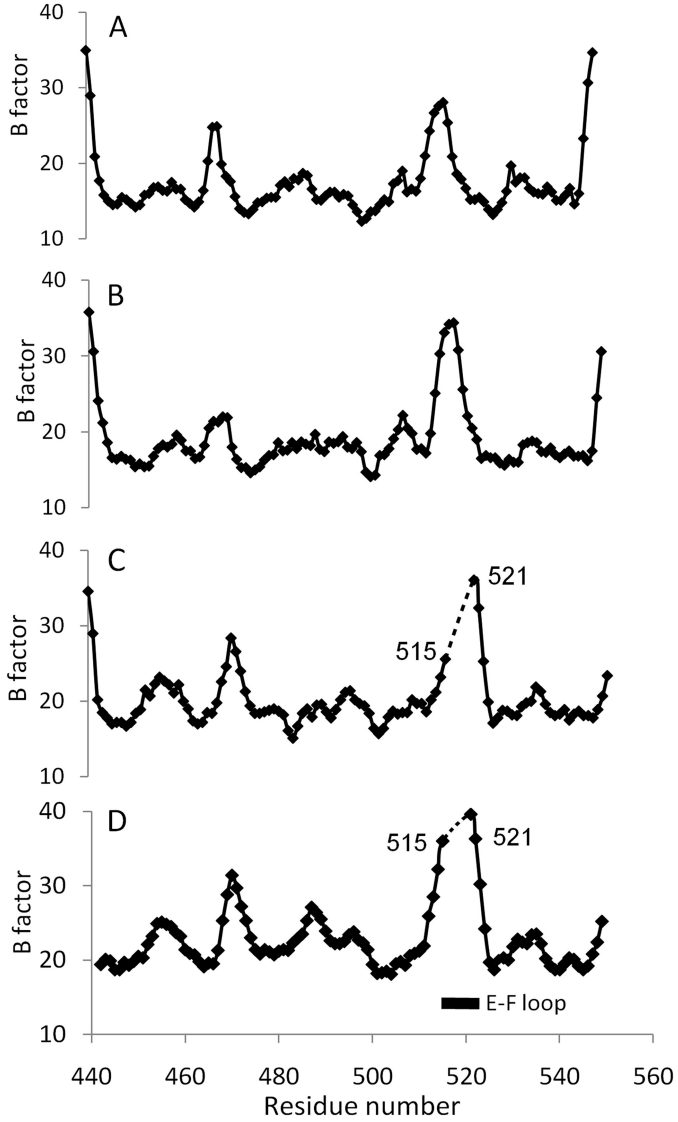

FIGURE 3. **Thermal B values *versus* residues in each monomer of an asymmetric unit of CALX-CBD1 structure.** *A*, monomer B; *B*, monomer A; *C*, monomer C; and *D*, monomer D.

TABLE 1
Data processing and model refinement statistics for CALX-CBD1 structures

	CALX-CBD1 Ca^{2+}-bound form	CALX-CBD1 apoform
Data collection		
Space group	$P2_12_12_1$	$P2_12_12_1$
Unit cell (Å)	59.4, 73.7, 129.7	59.1, 76.5, 129.0
Wavelength (Å)	1.90	1.00
Resolution range (Å)[a]	20–2.25 (2.3–2.25)	47.6–1.6 (1.70–1.60)
Observations (total/unique)	196,637/26,203	553,318/146,906
$I/\sigma(I)$[a]	14.1 (3.1)	15.6 (2.0)
Completeness (%)[a]	94.4 (71.8)	98.7 (95.8)
R_{sym} (%)[a]	7.2 (54.4)	10.7 (57.7)
Structure refinement		
R_{work}/R_{free}	20.8/26.5	19.2/22.1
Number of atoms[b]	3,596/16/120	3,482/6/461
r.m.s.d.[c] bond length (Å)	0.017	0.012
r.m.s.d. bond angle	1.76°	1.63°
Ramachandran analysis (%)		
Most favored	91.2	91.5
Additional favored	8.8	8.2
Generously allowed	0	0.3
B factors (average)		
Monomer A/B/C/D	47.7/45.3/46.1/62.3	20.4/18.7/21.2/23.2
Ca^{2+}	64.5	25.7
Water	39.1	32.1

[a] Values within parentheses refer to the high resolution shell.
[b] Non-hydrogen protein atoms/metal atoms/water molecules.
[c] r.m.s.d., root mean square deviation.

unchanged; they are stabilized by a hydrogen bond network with a water molecule at position 324.

Strikingly, both monomers C and D represent the true apoform, and no Ca^{2+} can be found in corresponding regions (Fig. 2*C*). Nearly all residues involved in Ca^{2+} binding become invisible, particularly the entire E–F loop (Asp^{516}–Glu^{522}), which strongly suggests that the primary Ca^{2+} pair plays a critical role in stabilizing the entire Ca^{2+} binding region. The disorder of the Ca^{2+} binding region has no impact on the overall β-sheet structure of CBD1 and the neighboring C–D loop containing Asp^{490} is still clearly resolved. Both Ca^{2+}-free forms superimpose well with similar root mean square deviation values of 0.44 Å for backbone atoms and 0.97 Å for all atoms. Notably, no Ca^{2+} binding region from these four monomers is involved in crystal packing, and all four monomers display comparable thermal B factors (Table 1 and Fig. 3).

Our structural observations indicate that no gross conformational changes occur during Ca^{2+} binding. To exclude any possible effects of crystallization constraints, the Ca^{2+} extraction experiment was performed in solution with monitoring by CD spectroscopy. The result shows CBD1 protein exhibits a full β-strand conformation, as expected (Fig. 4*A*). No detectable change of protein secondary structure was observed by addition of either 2 mM Ca^{2+} (Fig. 4*B*) or 10 mM EDTA (Fig. 4*C*). Notably, 10 mM EDTA causes Ca^{2+} unbinding of CBD1 of NCX1 (8).

Mutational Analysis of Ca^{2+} Binding Site of CBD1—Two residues, Glu^{455} and Glu^{520}, are involved in the coordination of three Ca^{2+} at the CBD1 site, although they differ in the specific Ca^{2+} ions which are involved (Glu^{455} with Ca-1, -2, and -3; Glu^{520} with Ca-2, -3, and -4). Our structural data suggest that Glu^{455}, which coordinates the primary Ca^{2+} pair, plays a more important role in stabilizing the entire Ca^{2+} binding region than Glu^{520}. To examine whether these two glutamate residues have unequal functions in the Ca^{2+}-dependent regulatory mechanism, they were mutated into Asp and/or Ala. RNA from either the wild-type CALX1.1 or various mutant exchangers was injected into *Xenopus laevis* oocytes, and the outward currents were recorded to evaluate functional Ca^{2+} regulation. The overlapping traces in Fig. 5*A* show representative outward Na^+-Ca^{2+} exchange currents for wild-type CALX1.1 at four different Ca^{2+} concentrations. In the absence of regulatory Ca^{2+}, CALX is fully activated by the application of 100 mM Na^+. However, both peak and steady-state currents become substantially suppressed by increasing the concentration of regulatory Ca^{2+}. (Results obtained at 1, 3, and 10 μM are shown.) The corresponding IC_{50}s for peak and steady-state currents are 0.4 ± 0.1 μM and 0.13 ± 0.002 μM, respectively.

Even though Glu^{520} appears to have the equivalent Ca^{2+} coordinating capacity as Glu^{455} (*i.e.* three Ca^{2+}), it exhibits far less importance in mediating the Ca^{2+} regulatory response. Mutations of these two residues illustrate their different functional roles. The Ca^{2+} dependence of peak and steady-state currents of these mutants are presented in Fig. 5, *E* and *F*. In the

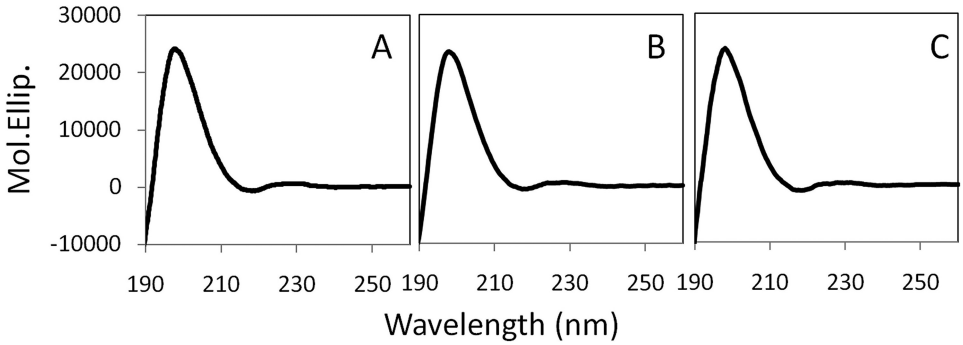

FIGURE 4. **CD spectra of CALX-CBD1 upon Ca^{2+} binding.** *A*, CBD1 protein after the protein purification; *B*, the CBD1 protein with 2 mM Ca^{2+}; and *C*, the CBD1 protein with 10 mM EDTA.

E520A mutation, there is only a slight reduction in the inhibitory potency of regulatory Ca^{2+} for peak currents, (IC_{50}s = 1.2 ± 0.01 μM) and even less for steady-state currents (0.22 ± 0.06 μM) (Fig. 5*B*).

In sharp contrast, the Ca^{2+} response is much more sensitive to changes at residue Glu^{455}. The E455A mutation results in a dramatic alteration of the Ca^{2+} regulatory response. Both peak and steady-state currents are not appreciably inhibited until the level of regulatory Ca^{2+} reaches 3 μM (Fig. 5*D*). The apparent Ca^{2+} affinity of E455A for regulation of peak currents is reduced by ~20-fold to IC_{50} = 8.1 ± 0.5 μM. Steady-state currents show an even greater reduction in the inhibitory potency of regulatory Ca^{2+}, which drops by 35-fold to 3.5 ± 0.2 μM. We also mutated Glu^{455} to an Asp. Similar to E455A, as shown in Fig. 5*C*, this conservative mutant shows a large shift in the affinity for functional Ca^{2+} regulation, which now appears at the level of 1 μM Ca^{2+}. The inhibitory potency of regulatory Ca^{2+} is reduced by nearly ~17-fold for both peak (6.7 ± 1.3 μM) and steady-state currents (1.7 ± 0.1 μM). These results clearly demonstrate that residue Glu^{455} is essential for Ca^{2+} binding and ultimately the transduction of the regulatory Ca^{2+} binding signal. The integrity of Glu^{455} is critical in maintaining normal exchanger regulation of CALX.

DISCUSSION

Ca^{2+} interactions occurring at CBD1 are essential for properly controlling sodium-calcium exchange activity and for the maintenance and reestablishment of resting Ca^{2+} levels in living cells. In this study, the Ca^{2+}-bound structure of CALX-CBD1 precisely confirms the occupancy of four Ca^{2+} within this site by their anomalous signals. Our data shows that CALX has a similar overall structure and Ca^{2+} binding site of CBD1 as does the mammalian NCX1, irrespective of their opposite Ca^{2+} regulatory phenotypes. Therefore, Ca^{2+} binding within the CBD1 structures likely represents a general mechanism within the larger NCX family.

Despite the nearly identical sequence composition of the Ca^{2+} binding sites within CBD1 from either CALX or NCX1, both the Ca^{2+}-bound and apoform CALX-CBD1 structures consistently demonstrate that Glu^{455} in the core of the Ca^{2+} binding site plays a significantly different role in Ca^{2+} coordination compared with Glu^{385} in the NCX1 structure. Possibly, this difference between CALX and NCX1 could be attributed to the lower resolution (2.5 Å) of the NCX1 structure (11). The oxygen atoms of the carboxylate group of Glu^{385} were not well defined, as seen in the electron density of the NCX1 structure. To date, no mutations of Glu^{385} in NCX1 have been reported. Given the remarkable impact of Glu^{455} mutations, we would predict that this Glu residue plays an important role in the Ca^{2+} regulatory mechanism of mammalian NCX1 and other exchanger proteins.

All characterized exchangers show concentration-dependent Ca^{2+} regulatory effects. For example, CALX, as seen in Fig. 5*A*, responds in a graded manner to the progressive administration of regulatory Ca^{2+}. In contrast to NCX1-CBD2 (8, 10), CALX-CBD2 does not have Ca^{2+} binding capabilities (7). CBD1 is the only Ca^{2+} binding region within the entire Ca^{2+} regulatory domain that could be responsible for this progressive negative Ca^{2+} regulatory phenotype. Therefore, the graded Ca^{2+} regulation exhibited in Fig. 5*A* must represent regulatory Ca^{2+} binding at CBD1. However, with only Ca^{2+}-bound structures, previously reported for CBD1 (8, 11), it is impossible to distinguish whether Ca^{2+} regulation at the level of a single exchanger protein constitutes an all-or-none *versus* a graded Ca^{2+} binding phenomenon.

In this study, we determined the apoform structure of CBD1 as well as that of an intermediate with two, rather than four, Ca^{2+} bound. The apoform structure clearly indicates that the primary Ca^{2+} pair is critical for the stabilization of the entire Ca^{2+} binding site of CBD1 whereas the effect of the secondary Ca^{2+} pair is quite modest. This is consistent with our functional analysis, where mutations that altered Glu^{455} (coordinating the primary Ca^{2+} pair) strongly disrupted Ca^{2+} regulation, whereas mutations of Glu^{520} (coordinating the secondary Ca^{2+} pair) only resulted in subtle reductions of Ca^{2+} affinity. These two Ca^{2+} pairs also interact with other carboxylate groups (Fig. 1*B*). Given the modest effect of the other carboxylate residues in the Ca^{2+} binding site of CBD1 suggested by a previous mutagenesis study (15), the affinity of E520A mutant (0.13 μM) or E455A (3.5 μM) should approximate the affinities for the primary Ca^{2+} pair or the secondary Ca^{2+} pair, respectively. Calcium concentrations of 0.13–3.5 μM would correspond to the reactive concentration range of regulatory Ca^{2+} for CBD1. In the dynamic Ca^{2+} environment of living cells, the primary Ca^{2+} pair with its higher affinity is expected to access CBD1 initially to establish the conformational transitions. These observations clearly elucidate that the four Ca^{2+} access the binding site of CBD1 in a sequential manner, rather than by simultaneous occupation.

The mechanism through which occupancy of the CBDs by Ca^{2+} is ultimately transduced to the transport machinery within the TM segments remains unknown. A plausible theory would be that substantial conformational changes occur upon Ca^{2+} binding, which are subsequently transmitted to the transport machinery. In fact, a fluorescent resonance energy transfer

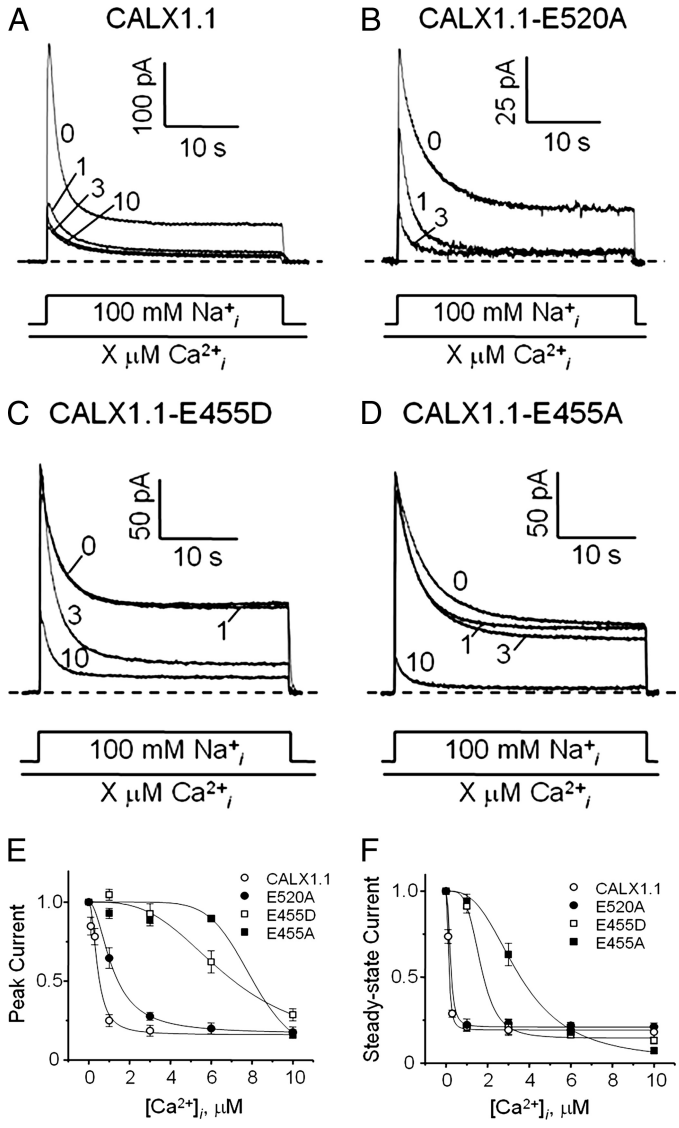

FIGURE 5. **Representative outward Na^+/Ca^{2+} exchange currents showing the regulatory Ca^{2+} dependence of the wild-type and various CALX1.1 mutant exchangers.** 8 mM Ca^{2+} was present in the pipette, and the currents were activated by the addition of 100 mM Na^+ to the cytoplasmic surface of the patch with regulatory Ca^{2+} absent or present at various concentrations. For wild-type (*A*), E455D (*C*) and E455A (*D*), exchange currents were recorded at four different Ca^{2+} concentrations (0, 1, 3, and 10 μM) as indicated. For E520A (*C*), only three different Ca^{2+} concentrations (0, 1, and 3 μM) were tested. $Ca^{2+}{}_i$ dependence of pure outward currents for peak (*E*) and steady state (*F*) mediated by wild-type CALX1.1 and various mutants. Currents were normalized to those obtained at 0 $Ca^{2+}{}_i$ within the same patch. Data points were averaged from four to seven individual patches. IC_{50} for peaks: 0.4 ± 0.1, 1.2 ± 0.01, 6.7 ± 1.3, and 8.1 ± 0.5 μM Ca^{2+} for CALX1.1, E520A, E455D, and E455A, respectively. IC_{50} for steady-state currents: 0.13 ± 0.002, 0.22 ± 0.06, 1.7 ± 0.1, and 3.5 ± 0.2 μM Ca^{2+} for CALX1.1, E520A, E455D, and E455A, respectively.

study with NCX1 indicated that Ca^{2+} binding elicits a conformational change of CBD1 (26). The apoform structure shows that CBD1 maintains the integrity of its β-sandwich conformation regardless of Ca^{2+} binding, whereas conformational changes caused by Ca^{2+} interactions are limited to the residues in the Ca^{2+} binding region as examined by CD spectroscopy and x-ray crystallography, arguing that a change of quaternary structure of CBD1 is not a requirement for the Ca^{2+} regulatory mechanism. Occupancy by the primary Ca^{2+} pair only affects

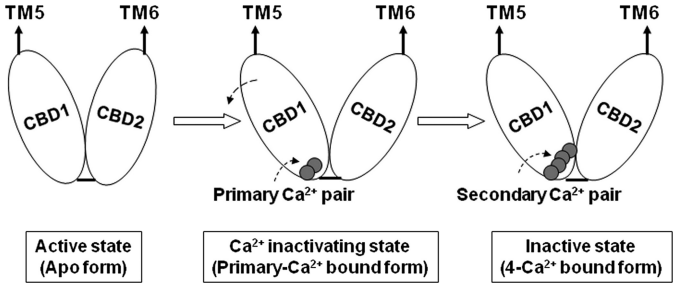

SCHEME 1. **Hypothetical mechanism of Ca^{2+} regulation for the CALX Na^+/Ca^{2+} exchanger.**

the stabilization of the Ca^{2+} binding site, especially within the E–F loop, as has also been shown for NCX1-CBD1 by NMR (12). Considering the fact that the E–F loop locates to the CBD1 domain surface, we propose that the Ca^{2+} binding signal is transduced from the E–F loop by communication to adjacent domain(s).

For all NCX proteins, the C terminus of CBD1 must connect with the N terminus of CBD2 in a very compact manner, providing the strong possibility that the Ca^{2+} binding site, particularly the E–F loop of CBD1, interacts with the N-terminal region of CBD2. Our mutational analysis shows that carboxylate residues in the Ca^{2+} binding sites of CBD1 serve unequal roles in the Ca^{2+} regulatory mechanism (Fig. 5). Notably, the essential residue Glu^{455} locates very close to the link or hinge region, further supporting the possibility that the signal of Ca^{2+} binding is transduced through this link via domain interactions between CBD1 and CBD2. This possibility is also strongly supported by our previous mutational analysis, where a proline mutation of Gly^{555} completely eliminated the Ca^{2+} regulatory properties of CALX (15). This proline mutation occurs at the joint between CBD1 and CBD2 and presumably disrupts CBD domain interactions.

Overall, our results support a mechanistic hypothesis that Ca^{2+} binding/unbinding at CBD1 is transduced through the interdomain interactions between the Ca^{2+} binding sites of CBD1 and CBD2 and that the E–F loop of CBD1 acts as a hinge for this domain interaction. As a consequence, Ca^{2+} binding at CBD1 stabilizes the E–F loop and in turn changes the orientation between these two rigid domains to influence the motion, ion access, or functionality of the transmembrane segments. Given that similar effects are also reported for the analogous mutation, G503P, in NCX1 (9), this general Ca^{2+} regulatory mechanism may also be applicable to the larger Na^+/Ca^{2+} exchanger protein family.

Based on our structural and functional analysis, we hypothesize that the Ca^{2+} regulatory mechanism occurring via CBD1 for CALX is performed in two sequential steps, as follows (Scheme 1): 1) CALX remains fully active when CBD1 exists in its apoform; 2) the primary pair of Ca^{2+} ions accesses the binding site to stabilize the E–F loop and alters the domain orientation angle between CBD1 and CBD2, generating a conformational change of the TM segments to initiate transporter inactivation; 3) as the Ca^{2+} concentration increases, the secondary Ca^{2+} pair binds to CBD1, stabilization of the E–F loop is further enhanced, and the TM transport machinery becomes more completely inactivated by stabilization of this inactive

state. Notably, such notions are becoming increasingly testable based on existing structure-function studies.

The graded nature of Ca^{2+} regulatory effects are even more pronounced for NCX1 than for CALX. In NCX1, Na^{+}/Ca^{2+} exchange currents are triggered by submicromolar Ca^{2+} levels and are amplified almost continuously by higher Ca^{2+} levels exceeding 10 μM, presumably in response to the much larger changes in intracellular Ca^{2+} levels that occur in cardiac myocytes. Our structures provides solid evidence that stepwise regulation of exchange is accomplished through different Ca^{2+} binding states in the CBD1 domain through its communication between the two CBDs. Very recently, a comparably functional study with NCX1 CBD1 mutants supports further application of our hypothetic model (28). Additional understanding of this interplay will need to be addressed by future crystallographic studies of the entire intracellular loop in conjunction with mutagenesis studies.

Acknowledgments—We thank Magnus Hook for assistance with CD analyses, Joachim Diez at Swiss Light Source for help with data collection, and John L. Spudich for valuable discussion on the manuscript.

REFERENCES

1. Bers, D. M. (1991) *Excitation-Contraction Coupling and Cardiac Contractile Force*, pp. 71–92, Kluwer Academic Publications, London
2. Blaustein, M. P., Fontana, G., and Rogowski, R. S. (1996) *Ann. N.Y. Acad. Sci.* **779,** 300–317
3. Linck, B., Qiu, Z., He, Z., Tong, Q., Hilgemann, D. W., and Philipson, K. D. (1998) *Am. J. Physiol.* **274,** C415–C423
4. Nicoll, D. A., Ottolia, M., and Philipson, K. D. (2002) *Ann. N.Y. Acad. Sci.* **976,** 11–18
5. Matsuoka, S., Nicoll, D. A., Reilly, R. F., Hilgemann, D. W., and Philipson, K. D. (1993) *Proc. Natl. Acad. Sci. U.S.A.* **90,** 3870–3874
6. Schwarz, E. M., and Benzer, S. (1997) *Proc. Natl. Acad. Sci. U.S.A.* **94,** 10249–10254
7. Wu, M., Wang, M., Nix, J., Hryshko, L. V., and Zheng, L. (2009) *J. Mol. Biol.* **387,** 104–112
8. Hilge, M., Aelen, J., and Vuister, G. W. (2006) *Mol. Cell* **22,** 15–25
9. Matsuoka, S., Nicoll, D. A., Hryshko, L. V., Levitsky, D. O., Weiss, J. N., and Philipson, K. D. (1995) *J. Gen. Physiol.* **105,** 403–420
10. Besserer, G. M., Ottolia, M., Nicoll, D. A., Chaptal, V., Cascio, D., Philipson, K. D., and Abramson, J. (2007) *Proc. Natl. Acad. Sci. U.S.A.* **104,** 18467–18472
11. Nicoll, D. A., Sawaya, M. R., Kwon, S., Cascio, D., Philipson, K. D., and Abramson, J. (2006) *J. Biol. Chem.* **281,** 21577–21581
12. Johnson, E., Bruschweiler-Li, L., Showalter, S. A., Vuister, G. W., Zhang, F., and Brüschweiler, R. (2008) *J. Mol. Biol.* **377,** 945–955
13. Hryshko, L. V., Matsuoka, S., Nicoll, D. A., Weiss, J. N., Schwarz, E. M., Benzer, S., and Philipson, K. D. (1996) *J. Gen. Physiol.* **108,** 67–74
14. Wang, T., Xu, H., Oberwinkler, J., Gu, Y., Hardie, R. C., and Montell, C. (2005) *Neuron.* **45,** 367–378
15. Dyck, C., Maxwell, K., Buchko, J., Trac, M., Omelchenko, A., Hnatowich, M., and Hryshko, L. V. (1998) *J. Biol. Chem.* **273,** 12981–12987
16. Studier, F. W. (2005) *Protein Expr. Purif.* **41,** 207–234
17. Kabsch, W. (1993) *J. Appl. Cryst.* **26,** 795–800
18. McCoy, A. J., Grosse-Kunstleve, R. W., Adams, P. D., Winn, M. D., Storoni, L. C., and Read, R. J. (2007) Phaser crystallographic software. *J. Appl. Cryst.* **40,** 658–674
19. Murshudov, G. N., Vagin, A. A., and Dodson, E. J. (1997) *Acta Cryst.* **D53,** 240–255
20. Emsley, P., and Cowtan, K. (2004) *Acta Cryst.* **D60,** 2126–2132
21. Ten Eyck, L. F. (1973) *Acta Cryst.* **A29,** 183–191
22. DeLano, W. L. (2002) *The PyMOL Molecular Graphics System*. DeLano Scientific LLC, Palo Alto, CA
23. Zheng, L., Baumann, U., and Reymond, J. L. (2004) *Nucleic Acids Res.* **32,** e115
24. Omelchenko, A., Dyck, C., Hnatowich, M., Buchko, J., Nicoll, D. A., Philipson, K. D., and Hryshko, L. V. (1998) *J. Gen. Physiol.* **111,** 691–702
25. Bers, D. M., Patton, C. W., and Nuccitelli, R. (1994) *Methods Cell Biol.* **40,** 3–29
26. Ottolia, M., Philipson, K. D., and John, S. (2004) *Biophys. J.* **87,** 899–906
27. Hilge, M., Aelen J., Foarce, A., Perrakis, A., and Vuister, G. W. (2009) *Proc. Natl. Acad. Sci. U.S.A.* **106,** 14333–14338
28. Ottolia, M., Nicoll, D. A., and Philipson, K. D. (2009) *J. Biol. Chem.* **284,** 32735–32741